Dynamics of dual-fluorescent polymersomes with durable integrity in living cancer cells and zebrafish embryos

Askes, S.H.C.; Bossert, N.; Bussmann, J.; Talens, V.S.; Meijer, M.S.; Kieltyka, R.E.; ... ; Heinrich, D.M.

Citation
Askes, S. H. C., Bossert, N., Bussmann, J., Talens, V. S., Meijer, M. S., Kieltyka, R. E., ... Heinrich, D. M. (2018). Dynamics of dual-fluorescent polymersomes with durable integrity in living cancer cells and zebrafish embryos. *Biomaterials*, *168*, 54-63. doi:10.1016/j.biomaterials.2018.03.037

Version:	Publisher's Version
License:	Licensed under Article 25fa Copyright Act/Law (Amendment Taverne)
Downloaded from:	https://hdl.handle.net/1887/66399

Note: To cite this publication please use the final published version (if applicable).

https://openaccess.leidenuniv.nl

License: Article 25fa pilot End User Agreement

This publication is distributed under the terms of Article 25fa of the Dutch Copyright Act (Auteurswet) with explicit consent by the author. Dutch law entitles the maker of a short scientific work funded either wholly or partially by Dutch public funds to make that work publicly available for no consideration following a reasonable period of time after the work was first published, provided that clear reference is made to the source of the first publication of the work.

This publication is distributed under The Association of Universities in the Netherlands (VSNU) 'Article 25fa implementation' pilot project. In this pilot research outputs of researchers employed by Dutch Universities that comply with the legal requirements of Article 25fa of the Dutch Copyright Act are distributed online and free of cost or other barriers in institutional repositories. Research outputs are distributed six months after their first online publication in the original published version and with proper attribution to the source of the original publication.

You are permitted to download and use the publication for personal purposes. All rights remain with the author(s) and/or copyrights owner(s) of this work. Any use of the publication other than authorised under this licence or copyright law is prohibited.

If you believe that digital publication of certain material infringes any of your rights or (privacy) interests, please let the Library know, stating your reasons. In case of a legitimate complaint, the Library will make the material inaccessible and/or remove it from the website. Please contact the Library through email: OpenAccess@library.leidenuniv.nl

Article details

Askes S.H.C., Bossert N., Bussmann J., Talens V.S., Meijer M.S., Kieltyka R.E., Kros A., Bonnet S.A. & Heinrich D.M. (2018), Dynamics of dual-fluorescent polymersomes with durable integrity in living cancer cells and zebrafish embryos, Biomaterials 168: 54-63.
Doi: 10.1016/j.biomaterials.2018.03.037

Biomaterials 168 (2018) 54–63

Contents lists available at ScienceDirect

Biomaterials

journal homepage: www.elsevier.com/locate/biomaterials

Dynamics of dual-fluorescent polymersomes with durable integrity in living cancer cells and zebrafish embryos

Sven H.C. Askes [a], Nelli Bossert [b], Jeroen Bussmann [a], Victorio Saez Talens [a], Michael S. Meijer [a], Roxanne E. Kieltyka [a], Alexander Kros [a], Sylvestre Bonnet [a, *], Doris Heinrich [b, c, **]

[a] Leiden Institute of Chemistry, Leiden University, The Netherlands
[b] Leiden Institute of Physics, Huygens-Kamerlingh Onnes Laboratory, Leiden University, The Netherlands
[c] Fraunhofer Institute for Silicate Research, Würzburg, Germany

ARTICLE INFO

Article history:
Received 4 December 2017
Received in revised form
20 March 2018
Accepted 21 March 2018
Available online 22 March 2018

Keywords:
Nanovesicles
Amphiphilic block copolymer
Nanoparticle degradation
Intracellular trafficking
Fluorescence bio-imaging
Zebrafish embryos

ABSTRACT

The long-term fate of biomedical nanoparticles after endocytosis is often only sparsely addressed *in vitro* and *in vivo*, while this is a crucial parameter to conclude on their utility. In this study, dual-fluorescent polyisobutylene-polyethylene glycol (PiB-PEG) polymersomes were studied for several days *in vitro* and *in vivo*. In order to optically track the vesicles' integrity, one fluorescent probe was located in the membrane and the other in the aqueous interior compartment. These non-toxic nanovesicles were quickly endocytosed in living A549 lung carcinoma cells but unusually slowly transported to perinuclear lysosomal compartments, where they remained intact and luminescent for at least 90 h without being exocytosed. Fluorescence-assisted flow cytometry indicated that after endocytosis, the nanovesicles were eventually degraded within 7–11 days. In zebrafish embryos, the polymersomes caused no lethality and were quickly taken up by the endothelial cells, where they remained fully intact for as long as 96 h post-injection. This work represents a novel case-study of the remarkable potential of PiB-PEG polymersomes as an *in vivo* bio-imaging and slow drug delivery platform.

© 2018 Elsevier Ltd. All rights reserved.

1. Introduction

Like liposomes, polymersomes are spherical nanovesicles with a self-assembled membrane composed of synthetic amphiphilic block copolymers, of which the simplest form has one hydrophilic block and one hydrophobic block [1–5]. The synthetic nature of polymersomes allows for tuning the vesicle parameters, for example to reach higher membrane thickness than liposomes (up to 21 nm), 5–50 times higher mechanical resistance, lower membrane permeability of encapsulated compounds, and/or higher long-term stability in aqueous media [6]. As a consequence, polymersomes are exceptional encapsulating nanosystems that have attracted much attention for drug delivery and as optical markers in bio-imaging [3,7–15]. In principle, the thickness of their membrane and their large aqueous interior allows for loading them with high amounts of hydrophilic, hydrophobic, or amphiphilic luminescent probes, while the encapsulated dyes should remain protected from cellular degradation and exocytosis. Likewise, cells should be protected from the potential cytotoxic effects of the probes, provided the block copolymer molecules do not disassemble in a biological environment. As for liposomes and polymer nanoparticles, polymersomes allow for passive targeting of cancer tissues *in vivo* due to the enhanced permeation and retention effect (EPR) of tumors [16–18], possibly combined with active targeting by surface functionalization with cancer cell-targeting moieties [9,19,20]. Tuning of the nanovesicles' zeta-potential is an additional important factor that determines their fate in biological systems [21]. Polymersomes that are slowly degraded by the cell are useful for studying the uptake and trafficking of nanoparticles in the endo-lysosomal pathways [22–25]. The potential of polymersomes for bio-imaging and drug delivery has been investigated [3,9,10,12,21,26–34], but very few studies have paid attention to their uptake dynamics, long-term imaging, and breakdown *in vitro*

* Corresponding author. Leiden University, PO Box 9500, 2300 RA Leiden, The Netherlands.
** Corresponding author. Leiden Institute of Physics, Huygens-Kamerlingh Onnes Laboratory, Leiden University, The Netherlands.
E-mail addresses: bonnet@chem.leidenuniv.nl (S. Bonnet), heinrich@physics.leidenuniv.nl (D. Heinrich).

https://doi.org/10.1016/j.biomaterials.2018.03.037
0142-9612/© 2018 Elsevier Ltd. All rights reserved.

and *in vivo*, although these parameters are critical to conclude on the usability of polymersomes for biomedical applications.

In this study, we use a polyisobutylene-monomethyl polyethylene glycol (PiB-PEG-Me) block copolymer for the construction of nanometer-sized polymersomes [35]. Polyisobutylene (PiB) was chosen as hydrophobic block because it is a highly biocompatible polymer with high hydrophobicity, low permeability for small molecules (e.g. water), and high chemical resistance [36]. Moreover, it is approved by the FDA for food-related applications [36]. Polyethylene glycol (PEG) was chosen as hydrophilic block as it is the established standard for the surface functionalization of bioimaging systems. It is also recognized that polymersomes with polyethylene glycol-containing (PEG) block copolymers feature a maximum-density PEG brush on their surface, which in turn maximizes the *in vivo* stealthiness by evading the immune system [3,37]. Apart from our previous study [35], PiB-PEG based polymersomes in particular have not yet been investigated for luminescence bio-imaging.

Here we label PiB-PEG polymersomes with two different dyes emitting at two different wavelengths: on the one hand the membrane was labelled with a lipophilic blue-fluorescent probe (2,5,8,11-tetra(*tert*-butyl)perylene; TBP) and on the other hand the aqueous interior was labelled with a water-soluble orange-fluorescent probe (sulforhodamine B; SRB), see Fig. 1a. This double-doping with two different dyes allows to optically differentiate the membrane from the aqueous interior, and to study whether the vesicles remain intact after cellular uptake. In this case, SRB was selected as hydrophilic fluorescent probe because it is known to be rapidly cleared from the cell when it is released from liposomes [38]. TBP was selected because it is more securely incorporated inside the bilayer of liposomes and polymersomes compared to unsubstituted perylene [35,39]. Also, the absorption spectra of TBP and SRB do not overlap significantly, which allows for optical distinction between the location of the two chromophores. Additionally, both probes are cheap and easy to integrate into the polymersome. First, the dual-fluorescent polymersomes were physically characterized and their uptake and cytotoxicity in A549 lung carcinoma cells were investigated to screen the polymersomes for potential in cancer cell drug delivery and imaging. Second, the polymersomes were continuously imaged for multiple days to examine their transport inside the cells after endocytosis. Third, the long-term polymersome breakdown by the cells was investigated using fluorescence imaging and flow cytometry for two weeks. Finally, because the zebrafish embryo is an emerging standard to screen the *in vivo* behavior of nanoparticles [40–42], we followed the nanovesicles in this model for 96 h after intravenous injection.

2. Results and discussion

2.1. Polymersome preparation and characterization

A polyisobutylene-monomethyl polyethylene glycol (PiB-PEG-

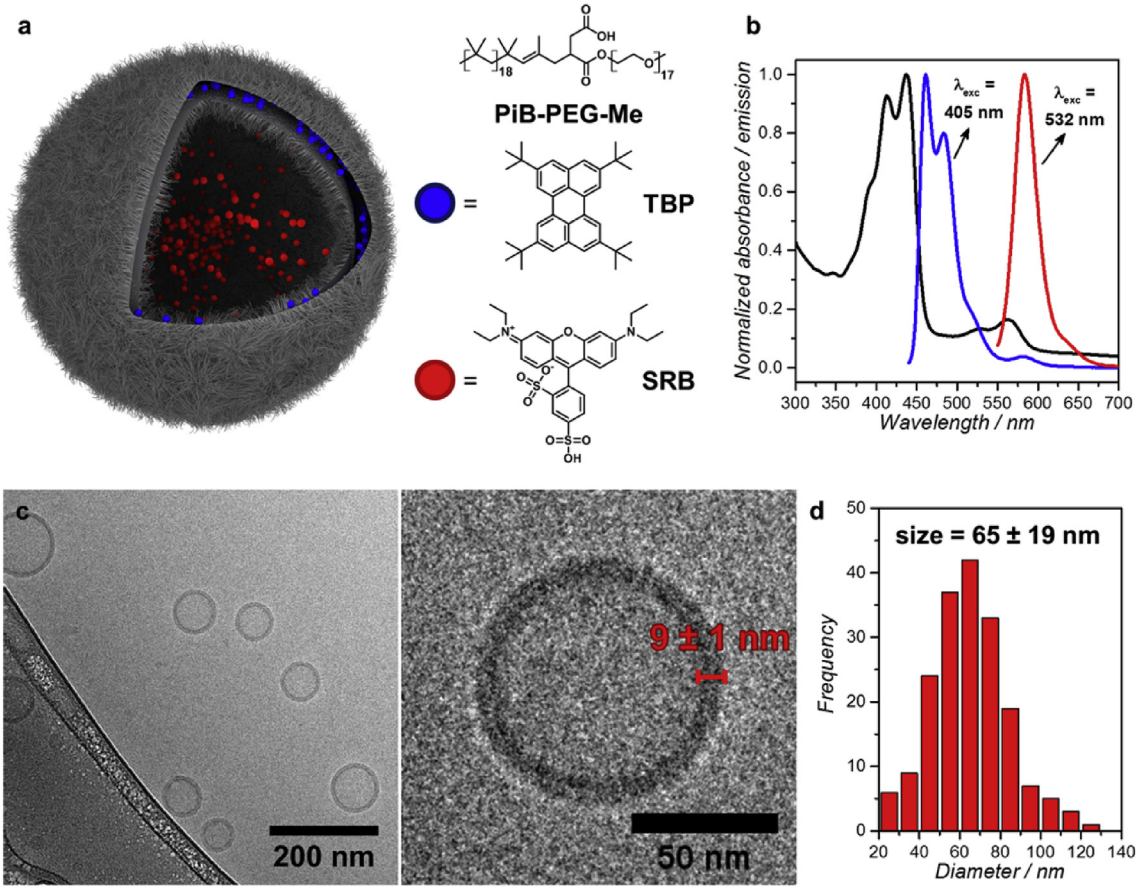

Fig. 1. Physical characterization of dual fluorescent polymersomes. a) Schematic representation of the dual fluorescent polymersomes and chemical structures of polyisobutylene-*block*-monomethyl polyethylene glycol copolymer (PiB-PEG-Me), 2,5,8,11-tetra(*tert*-butyl)perylene (TBP) and sulforhodamine B (SRB). b) Normalized absorption (black) and fluorescence spectra with $\lambda_{exc} = 405$ (blue curve) and 532 nm (red curve). c) Cryo-TEM micrographs (d) and size distribution of the particle diameter based on 186 individual vesicles. (For interpretation of the references to color in this figure legend, the reader is referred to the Web version of this article.)

Me) block copolymer was synthesized according to literature procedure with PiB and PEG block molecular weights of 1.0 and 0.75 kg mol^{-1}, respectively [35]. Dual-fluorescent polymersomes were then constructed by hydrating a dried polymer film containing 4 wt% blue-fluorescent 2,5,8,11-tetra(*t*-butyl)perylene (TBP) with phosphate buffered saline (PBS) containing 1.0 mM orange-fluorescent sulforhodamine-B (SRB). The polymersomes were subsequently sized by extrusion through a 0.1 μm pore filter membrane, and purified by removing the excess SRB using size-exclusion chromatography. The UV–Vis absorption spectrum of the resulting dispersion (Fig. 1b) showed the superposition of the individual absorption spectra of TBP ($\lambda_{abs} = 350–460$ nm) and SRB ($\lambda_{abs} = 500–580$ nm) [35], thereby confirming the presence of both chromophores in the nanovesicles. Interestingly, after three weeks of storage at room temperature neither SRB had escaped the aqueous interior nor TBP had escaped the membrane, as size-exclusion chromatography showed no free SRB or TBP elution band (data not shown). The fluorescence spectrum of freshly prepared polymersomes was then acquired with violet (405 nm) and green light excitation (532 nm). Under violet light excitation, the typical structured emission spectrum of TBP was observed between 450 and 550 nm. Only a small fluorescence signal of SRB was detected between 550 and 650 nm (4% of the total signal) due to the low absorbance of SRB at 405 nm. Under green light excitation, only SRB emission was observed, because TBP does not absorb above 450 nm. Thus, depending on excitation wavelength these polymersomes emit light either in the blue or in the orange region of the visible spectrum.

The average hydrodynamic diameter was determined using dynamic light scattering (DLS) in bulk solution, revealing a typical particle diameter of 97 nm with a polydispersity index of 0.19. These values did not change during 3 months of storage at 4 °C, representing exceptional stability in PBS. The zeta-potential was found to be negative (-39 ± 9 mV) due to the carboxylic acid at the block copolymer junction which is likely to be deprotonated in PBS. The individual particles were also visualized with cryo-TEM (Fig. 1c and d); the micrographs showed exclusively unilamellar polymersomes [43] with an average diameter of 65 ± 19 nm and a membrane thickness of 9 ± 1 nm, which is notably thicker than the 3–5 nm thick phospholipid bilayer of liposomes [44]. Considering that PEG chains are poorly visible in cryo-TEM images due to poor contrast with the vitrified water, and that the extended chain length of the PiB-block is approximately 4.5 nm (~36 C–C bonds, 109° bond angle), this result suggests that the opposing PiB chains in the membrane are organized end-to-end. Altogether, the ease of nanovesicle formation and dye doping, as well as the cost-effectiveness of the materials, make PiB-PEG-Me polymersomes excellent candidates as dual-fluorescent nanoprobes.

2.2. Endocytosis and cytotoxicity

Uptake of dual-fluorescent polymersomes by 2D cell monolayers was investigated. The A549 human lung carcinoma cell was selected because it is well-studied and frequently used for screening drugs and drug delivery systems [45–49]. A549 cells were incubated with polymersomes (5 μg mL^{-1}) for 2 h (without medium refreshment) and subsequently imaged with a confocal microscope in bright field mode and with 405 nm and 561 nm excitation (Fig. 2). The images showed colocalization of TBP and SRB fluorescence in localized spots throughout the cytoplasm, reminiscent of endo-lysosomal compartments of A549 cells [38,50–52]. Staining of lysosomes with Lysotracker Red revealed that the polymersomes indeed accumulated in lysosomes (Fig. S1), confirming uptake via the usual endocytosis pathways [53–55]. The colocalization of TBP and SRB fluorescence (Fig. 2d) clearly indicates that the encapsulated SRB had not leaked out and thus the nanovesicles remained intact inside the cells once they have been endocytosed. In repeated experiments at lower magnification and thus a bigger field of view, not all cells took up the particles in equal amounts, which possibly results from differences in cell cycle phase (Fig. S2) [50].

The dependence of cell viability on polymersome concentration was determined using a well-established cytotoxicity assay based on cell fixation and stoichiometric staining of cellular proteins (Fig. 2e) [45,56]. After incubation for 48 h, 50% cell viability was observed at a concentration of 0.5 mg/mL polymersomes, compared to untreated cells (Fig. 2e). No significant toxicity difference was observed between dual-fluorescent polymersomes and polymersomes that contained no dyes, thereby excluding toxic effects from the dyes themselves. Notably, although this assay yields a highly accurate quantification of the abundance of living cells, it does not incorporate numbers of dead cells. Microscopic screening of the cells in wells just before cell fixation showed that in each condition the cells displayed similar healthy states. However, it was obvious that a lower number of cells was observed when the polymersome concentration was increased, with no observation of varying cell death numbers. This leads to the conclusion that instead of causing cell death, the polymersomes rather exhibit a partially anti-proliferative effect. Overall, these initial results report fast uptake of the particles and low cytotoxicity, and prompted additional investigations in uptake dynamics and cellular tracking.

Polymersome endocytosis and transport within living cells was visualized during the first 2 h of incubation by confocal fluorescence microscopy. Additionally, the cells were stained with carboxyfluorescein succinimidyl ester (CFSE; $\lambda_{exc} = 488$ nm) to visualize the cell volume. Imaging was performed in bright field, and with 561 nm and 488 nm excitation every 5 s with 4 z-slices at each time point (Fig. 3 and Video V1). For these experiments, excitation with 405 nm was omitted because preliminary experiments indicated that the cells were quickly damaged by the near-UV light, consistent with reports that already blue light can be toxic to this cell line (50% cell death at 30 J cm^{-2} 455 nm irradiation) [45]. The polymersomes were added after 5 min of image acquisition. Within minutes after the start of incubation, the outer cell membrane was covered with numerous particles, randomly distributed across the membrane. After this initial docking, the particles began to move slowly and steadily towards the perinuclear area of the cell, thereby strongly suggesting the involvement of an active transport mechanism along the cytoskeleton. To further investigate the particles' motion in the first 2 h, the video was analyzed by single particle tracking (SPT) with ImageJ and the TrackMate plugin [57,58], to yield the particle trajectories and thus their tracking duration, distance, and mean particle velocity distributions (Figs. 3b and S3). The majority of the trajectories clearly directed towards the perinuclear area with a constant mean velocity of 2.4 ± 1.4 nm/s with trajectory distances up to 19 μm (based on 346 individually tracked particles, see Fig. S4). These results are rather curious, considering that early endosome motility in A549 cells is usually characterized by directional movements towards the nucleus with much higher average velocities (1–2 μm/s) and short speed bursts (4–6 μm/s) [59–63]. In our experiments, we observed only very few endocytosed particles exhibiting such highly dynamic behavior (Video V1). The slow intracellular trafficking may be caused by intracellular crowding, which slows down the active transport along the cytoskeleton. The directed movement towards the perinuclear area completed after about 1.5 h for the initial wave of endocytosed particles, after which the polymersomes were stationary. No subsequent movements towards the cell exterior were observed, indicating no exocytosis of the particles. After 2 h of incubation, the same cells were imaged with 405,

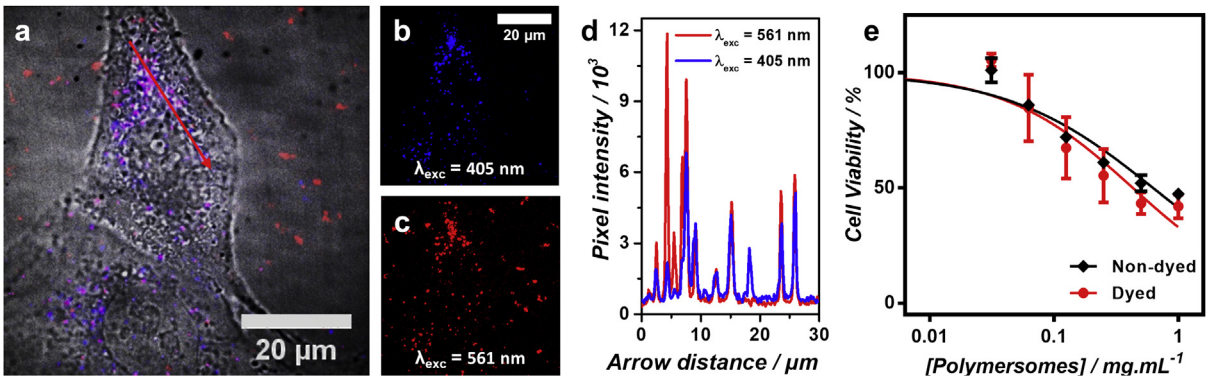

Fig. 2. Uptake and cytotoxicity of dual-fluorescent polymersomes. a,b,c) Confocal microscopy imaging of dual-fluorescent polymersomes in A549 cells after 2 h of incubation ([PiB-PEG-Me] = 5 µg/mL) in bright field mode and with λ_{exc} = 405 (blue; b) and λ_{exc} = 561 nm (red; c). The excess of polymersomes was not removed before imaging, hence free-floating vesicles are visible outside the cells. Each fluorescence channel constitutes a maximum intensity projection of the central 2 z-slices with 2 µm distance. d) Pixel intensities along the red arrow in (a) for λ_{exc} = 405 (blue) and λ_{exc} = 561 nm (red). e) Relative cell viability versus polymersome concentration (expressed as [PiB-PEG-Me] in mg/mL) of dyed (red circles) and non-dyed polymersomes (black diamonds) after 4 h incubation with polymersomes, medium refreshment, and a 48 h rest period. Error bars represent standard deviation based on three biological replications. Lines represent Hill-slope fits to the data. Uptake and transport dynamics visualized during the first 2 h of incubation. (For interpretation of the references to color in this figure legend, the reader is referred to the Web version of this article.)

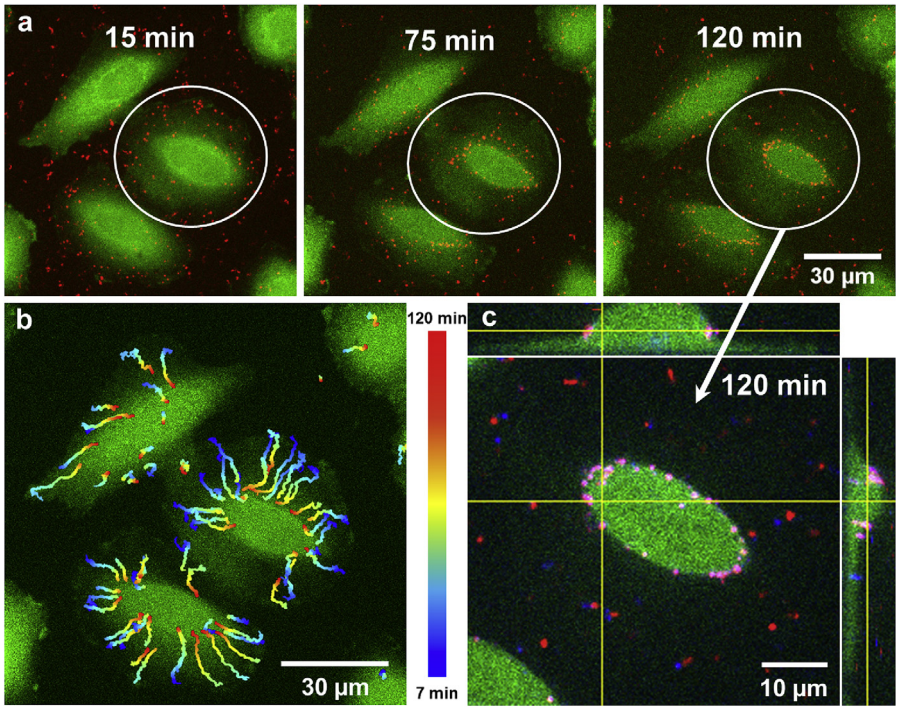

Fig. 3. a) Selected images from 2-h confocal fluorescence imaging of dual-fluorescent polymersomes (red, λ_{exc} = 561 nm) in living A549 cells that were stained with CFSE (green, λ_{exc} = 488 nm). The entire experiment is shown in Video V1. The vesicles were added at t = 5 min (50 µg/mL final concentration) and were not removed at any point. Each image constitutes a maximum intensity projection of 4 z-slices with 1.5 µm distance. b) Cells at 120 min (green) with single particle traces of 46 individual particles with the most long-lasting trajectories plotted. The traces are color-coded for the incubation time of the experiment as indicated next to the image. A larger dataset and the statistics are shown in the ESI. c) The circular region of interest in panel "a" was used for a detailed z-stack acquisition (0.3 µm z-slice distance) after 2 h of incubation with λ_{exc} = 405, 488, and 561 nm (blue, green, and red colors, respectively). One z-plane is shown, including the orthogonal xz and yz projections at the yellow lines. (For interpretation of the references to color in this figure legend, the reader is referred to the Web version of this article.)

488, and 561 nm excitation in a detailed z-stack (Fig. 3c). The colocalized fluorescence of TBP and SRB confirmed the presence of the intact dual-fluorescent polymersomes near the nucleus. Overall, the results show that the dual-fluorescent polymersomes are endocytosed by A549 cancer cells within the first minutes, followed by active but slow transport to the perinuclear area within 1.5 h.

Supplementary video related to this article can be found at https://doi.org/10.1016/j.biomaterials.2018.03.037.

2.3. Time-lapse imaging for 86 h

What is the fate of the nanovesicles after endocytosis and transport to the degradative environment of lysosomes? To answer this question, cells were incubated with a high dose of dual-fluorescent polymersomes for 4 h (0.5 mg ml^{-1} polymer), after which the cell medium was refreshed. Then, the cells were imaged every 2 min for 86 h in bright field and with 561 nm excitation

(Fig. 4 and Video V2), after which full cell confluency was reached. At the start of the experiment, most of the polymersomes were located nearby the nucleus, similar to the situation after 2 h incubation. During the next 86 h, the cells exhibited locomotion and mitosis, with no indications that the polymersomes caused cell death. This is consistent with our previous hypothesis that the polymersomes only slow down the cell division (see above). Each time a cell divided, the polymersomes were equally distributed among the two daughter cells (Video V2, Fig. S5). On this timescale, it was observed how polymersomes were dynamically shuttled throughout the cytosol, while most fluorescence was observed near the nucleus. No free-floating polymersomes were observed in solution directly above and near the cells. Moreover, the total SRB fluorescence did not decrease with time (based on data at 5 different locations, Fig. S6). These observations indicate that (i) SRB did not photobleach, (ii) the polymersomes were not exocytosed, (iii) and stayed intact inside the cells. To fully confirm this hypothesis, the cells were imaged after 90 h in bright field and with 405 and 561 nm excitation (Fig. 4b). Here again complete colocalization of TBP and SRB fluorescence was obtained, indicative of intact nanovesicles.

Supplementary video related to this article can be found at https://doi.org/10.1016/j.biomaterials.2018.03.037.

According to these experiments, these polymersomes were still completely intact after 90 h after uptake, which indicates that they are highly resistant towards cellular breakdown in the lysosomal pathway. We attribute this resistance to the high chemical inertness of the PiB polymer block [36]. On top of that, we have reported before that related PiB-PEG-Me polymersomes are mechanically tough, as they do not even burst in the high vacuum of a transmission electron microscope [35]. Altogether, we hypothesize that after endocytosis the polymersomes remain trapped in the endo-lysosomal pathways and are shuttled back and forth in these compartments. The unusually long dwelling time of the particles in the cells may originate from the fully PEGylated surface of the nanovesicles, which may obstruct the recognition of the particles and allows them to be present inside the lysosomes as camouflaged objects.

2.4. Long-term monitoring of polymersomes in cells during 11 days after incubation

The exceptional stability of these polymersomes in a 90 h experiment encouraged us to investigate how long the polymersomes would remain intact during a still longer experiment of 11 days. However, as cancer cells have a high proliferation rate, it was necessary to split the cell population several times within these 11 days to prevent over-confluency and concomitant cell death. Splitting of the population decreases the fluorescence signal per cell significantly in time, but the relative fluorescence intensity of one probe compared to the other provides information about the integrity of the particles. A549 cells were hence seeded 24 h before the experiment. On the starting day (day 0) a microscopy dish with the cells was incubated with 0.5 mg/mL dual-fluorescent polymersomes for 4 h, washed twice with PBS, and resupplied with growth medium. Directly afterwards, the cells were imaged with confocal microscopy. Subsequently, the cells were detached, in part reseeded in a new microscopy dish, and the excess of cells was analyzed by fluorescence flow cytometry (Fig. 5 and Fig. S7). This was repeated on days 3, 7, and 11.

The confocal microscopy images and their quantified fluorescence of TBP and SRB (Fig. 5a and b; N = 10 probing positions) showed that in the first 3 days after treatment, the polymersomes stayed inside the cells and that the fluorescence of both TBP and SRB remained unaffected. This is in accordance with our observations in Fig. 4. Between day 3 and 7, the fluorescence intensities of SRB and TBP greatly decreased per cell area, with only few intact polymersomes remaining. Many cells contained only TBP fluorescence, indicating that SRB had been degraded or had been exocytosed by the cell (close-ups in Fig. S8). On day 11, no fluorescence in either channel was observed anymore. Notably, at each imaging day, no fluorescent particles were observed that were moving around in the supernatant, i.e. directly above the cells, which suggests that exocytosis did not occur. The fluorescence flow

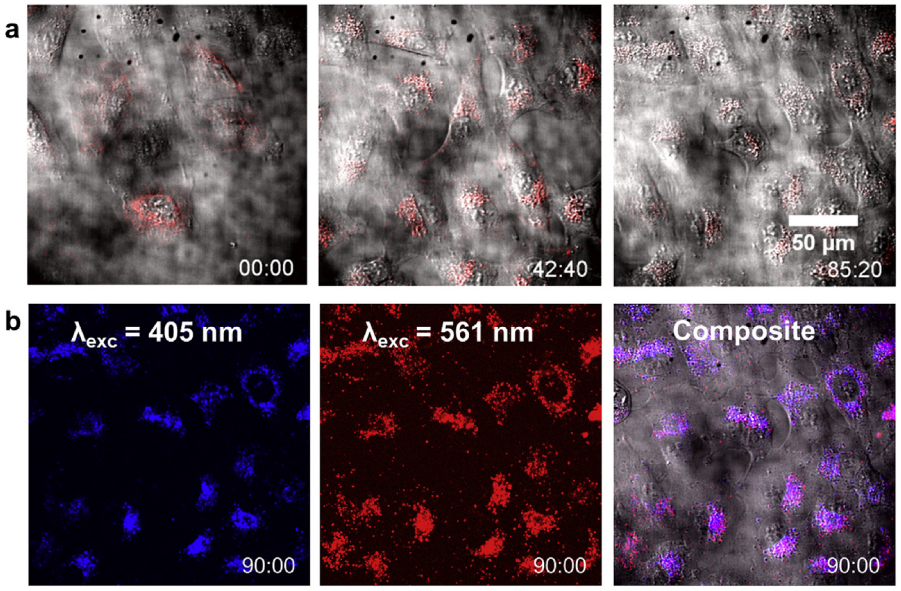

Fig. 4. Long-term time-lapse imaging. a) Selected images from 86 h confocal fluorescence imaging of dual-fluorescent polymersomes (red, $\lambda_{exc} = 561$ nm) in living A549 cells. Prior to imaging, the cells were incubated for 4 h with 0.5 mg/mL polymersomes, washed twice with PBS prior, and resupplied with Opti-MEM medium. Images were taken each 2 min; the entire experiment is shown in Video V2. Time is indicated in hour:minute format. b) Confocal images at 90 h after incubation. In all images the fluorescence channel constitutes a maximum intensity projection of 3 z-slices with 2 µm distance. (For interpretation of the references to color in this figure legend, the reader is referred to the Web version of this article.)

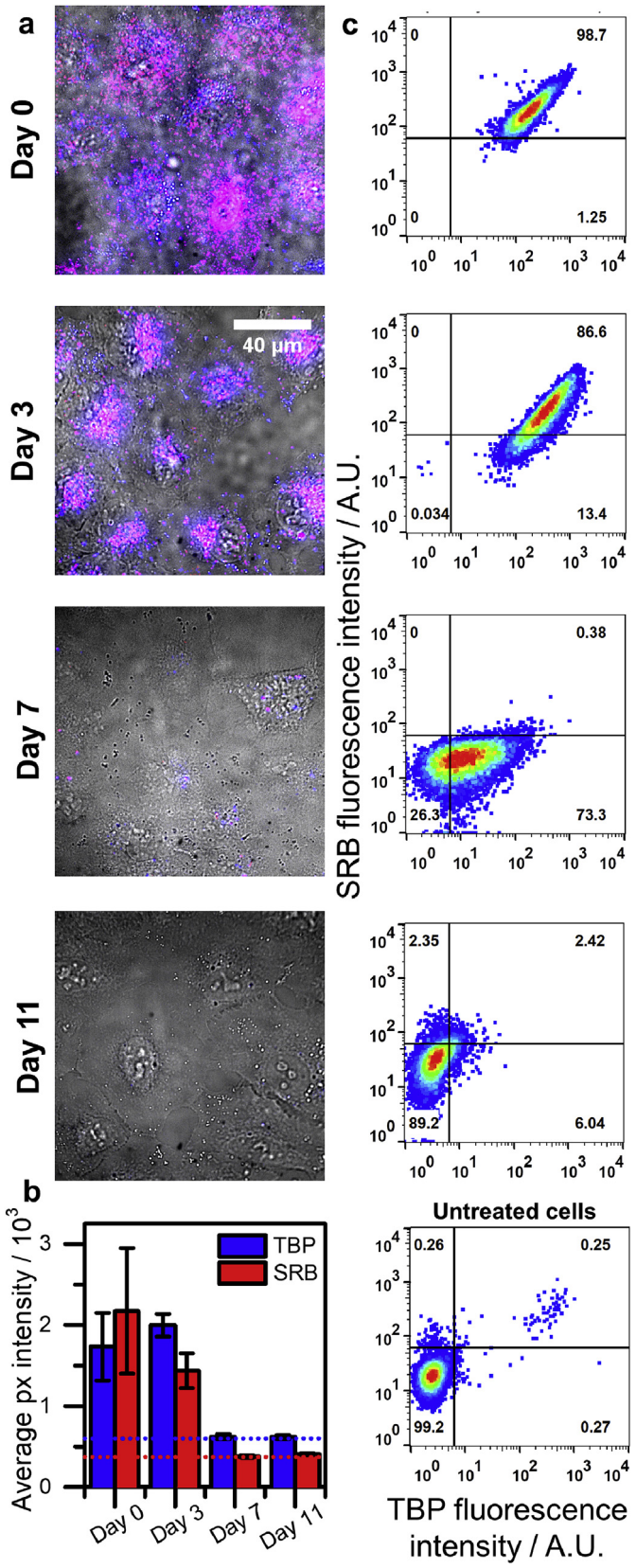

Fig. 5. Monitoring of A549 cells with endocytosed polymersomes for 11 days by fluorescence imaging and flow cytometry. a) Merged confocal bright field and fluorescence images of dual-fluorescent polymersomes (red, $\lambda_{exc} = 561$ nm; blue, $\lambda_{exc} = 405$ nm; purple showing colocalization) in living A549 cells at day 0 (directly after incubation and medium refreshment) and at day 3, 7, and 11. Each fluorescence image consists of a maximum intensity projection of 5 z-slices with 1.5 μm distance. For comparison, the TBP and SRB fluorescence histograms were equalized between datasets. b) Quantification of the fluorescence intensity per cell area (expressed in mean pixel value) under 405 (left) and 561 nm excitation (right) of 10 separate imaging areas (1 standard deviation error bar). Noise levels are indicated with blue and red dotted lines. c) Top to bottom: flow cytometry of the cells at day 0, directly after polymersome treatment, and at day 3, 7, and 11, and untreated cells (bottom). TBP and SRB fluorescence were collected with $\lambda_{exc} = 405/\lambda_{em} = 450 \pm 45$ nm and $\lambda_{exc} = 488/\lambda_{em} = 583 \pm 26$ nm, respectively. Cell population was selected by forward and side scatter (Fig. S7). The relative population (in %) is indicated per quadrant. (For interpretation of the references to color in this figure legend, the reader is referred to the Web version of this article.)

cytometry results followed the same trend as the imaging results: the fluorescence of TBP and SRB in the cell population evolved relatively little between day 0 and 3 (Fig. 5c). After 7 days, the signal of SRB was completely gone, while the TBP fluorescence remained. After 11 days, no more fluorescence was observed, comparable to untreated control cells. The fact that the SRB fluorescence disappeared before the TBP fluorescence suggests that SRB leaks out of the polymersomes between 3 and 7 days after incubation and that at this time only a collapsed polymer membrane remains, evident from the TBP fluorescence signal. This is further supported by the fact that the TBP fluorescence still originates from localized spots in the perinuclear area, *i.e.* lysosomes (Fig. S8). Further, the results suggest that between 7 and 11 days the remains of the polymer membrane are cleared by the cell and that TBP is degraded or excreted.

In order to investigate the mechanism behind degradation, the hydrodynamic size distribution of the polymersomes was measured during 10 days of incubation in *ex-vivo* conditions that mimic mammalian lysosomes, *i.e.* acidic environment (pH 4, 5, or 6), presence of digestive esterase enzymes [64], and human body temperature (37 °C; Fig. S9). Whereas incubation in acidic conditions alone did not result in any significant changes in size distribution (Fig. S9a), the presence of esterase enzyme resulted in agglomeration of the polymersomes, as observed by major increases in hydrodynamic size (Fig. S9b). This agglomeration was especially severe in combination with acidic conditions, e.g. from 100 nm on day 0–900 nm on day 10 for incubation at pH 4. The agglomeration is most likely the result of the enzymatic cleavage of the ester junction in the block copolymer, leading to dissociation of PEG from the polymersomes, destabilization of the lipid bilayer, and hydrophobic-hydrophobic attractions between "bare" PiB-rich polymersome fragments. Intriguingly, this enzymatic cleavage proceeds even in presence of the large steric hindrance of the PEG brush on the polymersome surface. The higher degree of agglomeration in more acidic conditions ($pH \leq 5$; Fig. S9b) can be explained by the neutralization of the resulting carboxylic acid moieties that remain on the cleaved PiB block, thereby removing any electrostatic repulsion between polymersome fragments. We thus conclude that an enzymatic degradation mechanism is responsible for the cellular degradation of dual-fluorescent polymersomes in mammalian cells. At this point, the fate of the individual polymer blocks after degradation remains unknown. Taken altogether, the data shows that the polymersomes remain stable inside the cells for up to 7 days without affecting cell survival. Moreover, the results suggest that the polymersomes are enzymatically degradable by cells within 3–7 days, with complete decomposition within 11 days. Such biocompatible properties are highly beneficial for bio-imaging nanoparticles that can be used for long-term imaging of cells and/or tissues: they can be introduced in a biological system and used to monitor specific areas for multiple days while in time they are naturally degraded. Alternatively, these degradable polymersomes can be filled with drugs for intracellular targeting, occurring within 3–7 days after uptake. In this scenario, a

water-soluble drug is initially trapped inside the vesicles due to the impermeability of the rubbery PiB bilayer, but enzymatic degradation of the block copolymer in time results in destabilization of the membrane and subsequent drug release.

2.5. Imaging of polymersomes in zebrafish embryos

Finally, to demonstrate the relevance of our *in-vitro* results for *in vivo* work, the dual-fluorescent polymersomes were imaged in a zebrafish embryo model, and their *in-vivo* toxicity was investigated. Here, the zebrafish embryo model was chosen because it has been recognized as emerging standard to screen the *in vivo* behavior of nanoparticles, due to the embryo's optical transparency, ease of fluorescence cell-labelling through genetic modification, and the broad applicability of drug delivery studies in this vertebrate model [40–42]. Transgenic zebrafish embryos, expressing green-fluorescent protein (GFP) in endothelial cells, were cultivated in order to allow fluorescence imaging of the vascular system. Zebrafish embryos were injected with 1 nL dual-fluorescent polymersomes (10 mg/mL) and monitored at 1, 8, 24, 48, and 96 h after injection using fluorescence microscopy, while the number of living fish were counted at each time point (Fig. 6 and Figs. S10–S14). As control, zebrafish embryos were injected with 1 nL PBS without polymersomes. At 1 h post-injection, the polymersomes had been endocytosed in endothelial cells, while no polymersomes were observed in the bloodstream. This is in agreement with previous results which show that particles with a negative zeta-potential are rapidly taken up in the endothelial cells of zebrafish embryos [42]. At 8, 24, 48, and 96 h post-injection, the situation remained completely unchanged: the colocalization of the fluorescence signal of TBP and SRB indicated that the nanovesicles remained completely intact and were neither excreted nor degraded. Meanwhile, none of the tested 92 zebrafish had died despite the relatively high number of injected nanoparticles. Although the nanovesicles should be rigorously tested for e.g. immunotoxicity and inflammatory response in additional studies, these observations suggest high biocompatibility of the dual-fluorescent polymersomes. Overall, these results demonstrate that PiB-PEG-Me polymersomes are (i) readily taken up by cells without subsequent exocytosis, (ii) not causing embryonic lethality within 96 h after injection, (iii) highly resistant towards cellular breakdown *in vivo* for at least 4 days, and (iv) a highly promising luminescent platform for long-term *in vivo* bio-imaging, which can be combined with targeted intracellular drug delivery. We propose that in future work, tuning the zeta-potential of the vesicles by (partial) methylation of the carboxylate groups may help to target different tissue types. For instance, vesicles with a longer blood circulation time may be beneficial for targeting cancer cells due to the enhanced permeability and retention effect (EPR). In addition, the surface of the nanovesicles may be functionalized with cancer cell-targeting moieties for long-term *in vivo* tumor imaging.

3. Conclusions

In conclusion, novel dual-fluorescent polyisobutylene-polyethylene glycol (PiB-PEG) polymersomes were prepared and used for long-term *in vitro* and *in vivo* bio-imaging. By doping both the hydrophilic interior and the lipophilic membrane of the polymersomes with two different fluorophores, information could be obtained regarding their integrity upon endocytosis. Polymersome uptake and intracellular transport dynamics studies revealed their quick endocytosis in less than 5 min. The nanovesicles were transported with a relatively slow velocity of about 2 nm s^{-1} along the endo-lysosomal pathway directly from the membrane to the perinuclear area, where they remained intact for at least 86 h. The investigation of the intracellular breakdown of the polymersomes showed the first effects on the integrity of the nanovesicles after 3–7 days and their absence and thus degradation by the cells after 7–11 days. *Ex-vivo* incubation in presence of esterase showed that enzymatic cleavage of the ester linker in the PiB-PEG block copolymer is most likely the initial step for intracellular breakdown of the polymersomes. At last, the nanovesicles were imaged in zebrafish embryos as *in vivo* model for 96 h, which revealed that the polymersomes showed no toxicity and are very suitable for long-term bio-imaging. Overall, this work demonstrates the intriguing interaction of PiB-PEG polymersomes with biological systems, and shows that they are an excellent particle system to host both lipophilic and hydrophilic chromophores while protecting these dyes from degradation by the cell for several days. Finally, this work is a novel study of the endocytosis and intracellular transport dynamics, biocompatibility, and breakdown of polymersomes *in vitro* and *in vivo*, and paves the way for the broader use of PiB-PEG based polymersomes in life science applications.

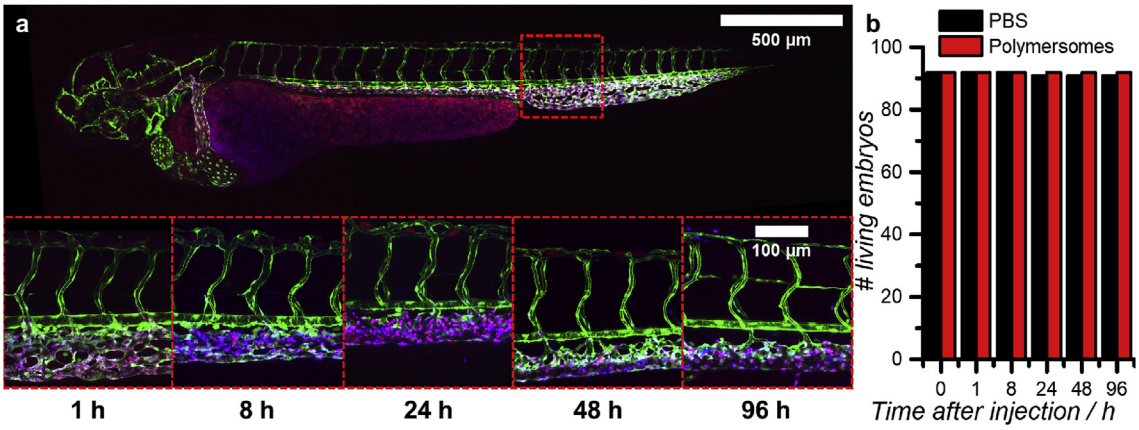

Fig. 6. *In vivo* luminescence imaging of dual-fluorescent polymersomes in zebrafish embryos. a) Fluorescence microscopy with 405 nm (blue), 488 nm (green) and 543 nm excitation (red) of kdrl:GFP transgenic zebrafish embryos at 1 h after injection with 1 nL dual-fluorescent polymersomes ([PiB-PEG-Me] = 10 mg/mL) and close-ups of the middle tail section (dashed red box) at 1, 8, 24, 48, and 96 h post-injection. Purple color indicates co-localization of TBP and SRB. b) Number of alive zebra-fish embryos at 1, 8,24, 48, and 96 h post-injection (N = 92 at t = 0) with dual-fluorescent polymersomes (red) and PBS as control (black). (For interpretation of the references to color in this figure legend, the reader is referred to the Web version of this article.)

4. Experimental

4.1. General

The chemical syntheses of PiB-PEG-Me and TBP are reported elsewhere [35]. Sulforhodamine B (SRB), porcine liver esterase (≥50 U/mg; 1 U corresponds to the amount of enzyme which hydrolyzes 1 μmol ethyl valerate per minute at pH 8.0 and 25 °C), and Dulbecco's phosphate buffered saline (PBS) were purchased from Sigma-Aldrich. DPBS had a formulation of 8 g/L NaCl, 0.2 g/L KCl, 0.2 g/L KH_2PO_4, and 1.15 g/L K_2HPO_4 with a pH of 7.1–7.5. The average hydrodynamic polymersome diameter and polydispersity index were measured with Dynamic Light Scattering (DLS) using a Zetasizer Nano S machine from Malvern Instruments Ltd., operating with a wavelength of 632 nm. The zeta potential measurements were carried out in a DTS1070 folded capillary cell in 9:1 Milli-Q H_2O:PBS at pH 7.1. All images and data were processed using Fiji ImageJ [65], Origin Pro, and/or Microsoft Excel software.

4.2. Preparation of dual-fluorescent polymersomes

Aliquots of chloroform stock solutions containing the polymersome constituents were added together in a flask to obtain a solution with 10 mg PiB-PEG-Me and 0.80 μmol TBP. The solvent was removed by rotary evaporation and subsequently under high vacuum for 15 min to create a polymer film on the flask wall. 1.0 mL PBS buffer containing 1 mM SRB was added and the polymer film was hydrated by 3 cycles of freezing the flask in liquid nitrogen and thawing in warm water (50 °C). The resulting clear dispersion was extruded 11 times through a Whatman Nuclepore 0.1 μm polycarbonate filter at room temperature using a mini-extruder from Avanti Polar Lipids, Inc. After extrusion, the SRB-loaded polymersomes were purified using an Illustra NAP-25 size exclusion column with Sephadex G25 packing (GE Healthcare). 1 mL sample was loaded on the column and eluted with 2 mL PBS. The yellow-purple elution band (~2 mL) was then collected and diluted with PBS to 10 mL volume to obtain the polymersomes at 1 mg/mL concentration. Finally, the polymersomes were sterilized by extrusion through a 0.2 μm syringe filter and stored under sterilized conditions before use in cell experiments.

4.3. Polymersome breakdown analysis in presence of acid and/or esterase

2 mL PBS dispersions were prepared that contained 0.1 mg/mL dual-fluorescent polymersomes and 0.13 mg/mL porcine liver esterase (≥50 U/mg), and were titrated with 1 M HCl to pH 4, 5, or 6, or left at pH 7. A second series of dispersions was made without esterase. The dispersions were incubated at 37 °C for 10 days while periodically measuring the hydrodynamic size distribution using DLS.

4.4. Cryo-TEM

A few microliters of a concentrated polymersome solution (10 mg/mL) was applied to a freshly glow-discharged Lacey Carbon Film Cu grid (300 mesh). The excess of liquid was blotted away for 2 s at room temperature at 95% humidity with a Whatman No. 4 filter paper and plunge-frozen in liquid ethane at −183 °C using a Leica EM GP automatic plunge freezer. Images of the vitrified samples were recorded under low dose conditions with a FEI Tecnai F20 FEG transmission electron microscope, equipped with a field emission gun at 200 kEV and a Gatan UltraScan camera, with a defocus between −3 and −6 μm.

4.5. General cell culturing

A549 human lung carcinoma cells were cultured in 25 cm^2 flasks in 8 mL Dulbecco's Modified Eagle Medium with phenol red (DMEM; Sigma Life Science, USA), supplemented with 8.2% v/v fetal calf serum (FCS; Hyclone), 200 mg/L penicillin and streptomycin (P/S; Duchefa), and 1.8 mM glutamine S (GM; Gibco, USA), under standard culturing conditions (humidified, 37 °C atmosphere containing 7.0% CO2). The cells were split approximately once per week upon reaching 70–80% confluency, using seeding densities of 2×10^5 cells, and the medium was refreshed once per week. Cells were passaged for 4–8 weeks.

4.6. Cell imaging preparation

For cell-imaging, after cell splitting the cells were suspended in OptiMEM (Life Technologies, USA), supplemented with 2.5% FCS, 200 mg/L P/S, and 1.8 mM GM. The cells were typically seeded in an IBIDI glass-bottom 8-well chamber-slide at $20–40 \times 10^3$ cells per well or in a 35 mm glass-bottom dish at $50–60 \times 10^3$ cells and incubated for 24 h before treatment. In the case of pre-incubation, the cells were incubated with a 1:1 v/v mixture of sterilized polymersomes and OptiMEM for 2 or 4 h at a typical concentration of 0.5 mg/mL. Then, the cells were washed once with PBS and resupplied with OptiMEM. In case of staining with carboxyfluorescein succinimidyl ester (CFSE), before imaging the cells were incubated with 10 μM CFSE for 20 min and washed twice with PBS, and resupplied with OptiMEM.

4.7. Live-cell imaging

Live-cell images were acquired on a Nikon Ti Eclipse inverted microscope (Nikon Corporation, Japan) equipped with a Yokogawa 10,000 rpm spinning disc unit (Andor Technology Ltd., United Kingdom) and a stage-top miniature incubation chamber (Tokai Hit, Japan; INUG2E-TIZ) with a TIZ-D35 sample holder mounted on a Nikon Ti–S-ER motorized stage. The cells were imaged with either a 40 × (Nikon Plan Fluor, numerical aperture (NA) 0.75), 60 × (Nikon Plan Apo λ, NA 1.4), or 100 × objective (Nikon SR Apo TIRF, NA 1.49). An Agilent MLC400B monolithic laser combiner (Agilent Technologies, Netherlands) was used for excitation at 405 nm, 488 nm and 561 nm in combination with a Semrock custom-made quad-band dichroic mirror for excitation wavelengths 400–410, 486–491, 460–570, and 633–647 nm. The emission was filtered using a Semrock quad-band fluorescence filter (TR-F440-521-607-700), which has specific transmission bands at 440 ± 40 nm, 521 ± 21 nm, and 607 ± 34 nm, or otherwise a Semrock TR-F447-060 for $\lambda_{exc} = 405$ nm or a Semrock TR-F607-036 for $\lambda_{exc} = 561$ nm. All images were captured by an Andor iXon Ultra 897 High-speed EM-CCD camera. Image acquisition was automated using NisElements software (LIM, Czech Republic). Typical exposure times per z-slice were 100–200 m s.

4.8. Flow cytometry experiments

24 h before the start of the experiment ("day 0"), four microscopy dishes were seeded with 60×10^3 A549 cells in OptiMEM complete medium. On day 0, the dishes were incubated with dual fluorescent polymersomes with an end concentration of 0.5 mg/mL for 4 h. Subsequently, the dishes were washed twice with PBS and resupplied with OptiMEM complete medium. One dish was used for confocal microscopy, another for flow cytometry after treatment with trypsin, and the remaining two were left in the incubator. On day 3, the latter two dishes were used for confocal microscopy and flow cytometry, while a part of the trypsinized cells was used for

seeding two new microscopy dishes (50×10^3 cells per dish). This was repeated on day 7 and 11. Fluorescence-assisted flow cytometry was performed on a Guava EasyCyte 12HT instrument equipped with 405 and 488 nm lasers. The blue fluorescence detection channel was 448 ± 50 nm and the orange fluorescence detection channel was 583 ± 26 nm. Finally, the data were analyzed and processed with FlowJo software. Cells and polymersomes were gated based on their forward and side scatter pattern (Fig. S7).

4.9. Cell cytotoxicity assay

The cytotoxicity of dual-fluorescent and undyed polymersomes was determined according to a reported protocol [45]. A549 lung carcinoma cells were seeded in the central 60 wells of a 96-well plate at 5 K cells per well in 100 μL Opti-MEM complete medium. 100 μL medium was added to every outer well. The plate was incubated for 24 h, after which 100 μL of polymersomes in PBS at different polymer concentrations (1.00, 0.500, 0.250, 0.125, 0.0625, and 0.0313 mg/mL) was added to the wells. Each condition was tested in triplicate. The outer wells and control wells were mock-treated with 100 μL PBS only. The plates were incubated for 4 h, after which the medium was refreshed with 200 μL Opti-MEM complete medium. After 48 h, the cells were fixed by adding 100 μL 10% wt./wt. trichloro acetic acid (TCA) in H_2O to each well and the plate was placed in a refrigerator at 4 °C for ca. 48 h. The TCA was removed by rinsing the plate gently with H_2O five times and drying the plate overnight at room temperature. Then, the inner 60 wells of the plate were stained with 100 μL sulforhodamine B (SRB, 0.6 wt% in 1 vol% acetic acid) for 30 min, after which the plate was washed five times in 1 vol% acetic acid. Once the plate was dry (±3 h), the SRB staining was dissolved in 200 μL 10 mM tris-base solution and the plate was placed on an orbital shaker for 30 min. Finally, the absorbance at 510 nm was measured with a plate reader (Tecan Infinite M1000 Pro) and the absorbance was converted to relative cell-viabilities using Microsoft Excel 2010 and GraphPad Prism 7 software. The data was fitted with a two-parameter Hill-slope equation which is used for obtaining the polymersome concentration at 50% relative cell viability [45]. The experiment was performed three times in three different weeks (*i.e.* three biological replicates).

4.10. Zebrafish embryo experiments

Zebrafish (*Danio rerio*, strain AB/TL) were maintained and handled according to the guidelines from the Zebrafish Model Organism Database (http://zfin.org) and in compliance with the directives of the local animal welfare committee of Leiden University. Fertilization was performed by natural spawning at the beginning of the light period and eggs were raised at 28.5 °C in egg water (60 μg/ml Instant Ocean sea salts). 1 nL polymersome solution (10 mg/mL) was injected into 2-day old *Tg(kdrl:GFP)*^{la116tg} zebrafish embryos (52–56hpf) using a modified microangraphy protocol [66]. Embryos were anesthetized in 0.01% tricaine and embedded in 0.4% agarose containing tricaine before injection into the sinus venosus/duct of Cuvier. Embryos were imaged 1, 8, 24, 48, and 96 h post-injection using a Zeiss LSM5 Exciter/Axio Observer confocal microscope at 10 × and 40 × magnification with 405, 488, and 543 nm excitation, while the viability of the embryos was assessed in a separate batch. The experiment was performed twice. In total, 92 embryos were used for the viability assessment.

Data availability

The raw/processed data required to reproduce these findings are available from the authors upon request.

Competing interests

Declarations of interest: none.

Acknowledgements

NWO (The Netherlands Organization for Scientific Research) is acknowledged for a VIDI grant to S·B and a VICI grant (724.014.001) to A.K. The European Research Council is acknowledged for an ERC starting grant to S.B. N.B. is funded by the NWO as part of the Frontiers of Nanoscience program. We thank Maria Götz (Fraunhofer ISC) for helpful discussions. We thank T.H. Sharp, R.I. Koning, and B. Koster (Leiden University Medical Center) for access to the cryoTEM facility and technical assistance.

Appendix A. Supplementary data

Supplementary data related to this article can be found at https://doi.org/10.1016/j.biomaterials.2018.03.037.

References

[1] D.E. Discher, F. Ahmed, Polymersomes, Annu. Rev. Biomed. Eng. 8 (1) (2006) 323–341.
[2] C. LoPresti, H. Lomas, M. Massignani, T. Smart, G. Battaglia, Polymersomes: nature inspired nanometer sized compartments, J. Mater. Chem. 19 (22) (2009) 3576–3590.
[3] A. Concheiro, C. Alvarez-Lorenzo, Smart Materials for Drug Delivery, Royal Society of Chemistry, Cambridge, 2013.
[4] J.P. Jain, W.Y. Ayen, N. Kumar, Self assembling polymers as polymersomes for drug delivery, Curr. Pharmaceut. Des. 17 (1) (2011) 65–79.
[5] D.E. Discher, A. Eisenberg, Polymer vesicles, Science 297 (5583) (2002) 967–973.
[6] H. Bermudez, A.K. Brannan, D.A. Hammer, F.S. Bates, D.E. Discher, Molecular weight dependence of polymersome membrane structure, elasticity, and stability, Macromolecules 35 (21) (2002) 8203–8208.
[7] J.V. Georgieva, R.P. Brinkhuis, K. Stojanov, C.A.G.M. Weijers, H. Zuilhof, F.P.J.T. Rutjes, D. Hoekstra, J.C.M. van Hest, I.S. Zuhorn, Peptide-mediated blood–brain barrier transport of polymersomes, Angew. Chem. Int. Ed. 51 (33) (2012) 8339–8342.
[8] R.J.R.W. Peters, M. Marguet, S. Marais, M.W. Fraaije, J.C.M. van Hest, S. Lecommandoux, Cascade reactions in multicompartmentalized polymersomes, Angew. Chem. Int. Ed. 53 (1) (2014) 146–150.
[9] T. Anajafi, S. Mallik, Polymersome-based drug-delivery strategies for cancer therapeutics, Ther. Deliv. 6 (4) (2015) 521–534.
[10] M.-H. Lai, S. Lee, C.E. Smith, K. Kim, H. Kong, Tailoring polymersome bilayer permeability improves enhanced permeability and retention effect for bioimaging, ACS Appl. Mater. Interfaces 6 (13) (2014) 10821–10829.
[11] P.P. Ghoroghchian, P.R. Frail, K. Susumu, D. Blessington, A.K. Brannan, F.S. Bates, B. Chance, D.A. Hammer, M.J. Therien, Near-infrared-emissive polymersomes: self-assembled soft matter for in vivo optical imaging, Proc. Natl. Acad. Sci. U.S.A. 102 (8) (2005) 2922–2927.
[12] M. Massignani, I. Canton, T. Sun, V. Hearnden, S. MacNeil, A. Blanazs, S.P. Armes, A. Lewis, G. Battaglia, Enhanced fluorescence imaging of live cells by effective cytosolic delivery of probes, PLoS One 5 (5) (2010) e10459.
[13] Z. Deng, Y. Qian, Y. Yu, G. Liu, J. Hu, G. Zhang, S. Liu, Engineering intracellular delivery nanocarriers and nanoreactors from oxidation-responsive polymersomes via synchronized bilayer cross-linking and permeabilizing inside live cells, J. Am. Chem. Soc. 138 (33) (2016) 10452–10466.
[14] G. Liu, X. Wang, J. Hu, G. Zhang, S. Liu, Self-immolative polymersomes for high-efficiency triggered release and programmed enzymatic reactions, J. Am. Chem. Soc. 136 (20) (2014) 7492–7497.
[15] X. Wang, G. Liu, J. Hu, G. Zhang, S. Liu, Concurrent block copolymer polymersome stabilization and bilayer permeabilization by stimuli-regulated "traceless" crosslinking, Angew. Chem. Int. Ed. 53 (12) (2014) 3138–3142.
[16] M. Ferrari, Cancer nanotechnology: opportunities and challenges, Nat. Rev. Canc. 5 (3) (2005) 161–171.
[17] Y. Matsumura, H. Maeda, A new concept for macromolecular therapeutics in cancer chemotherapy: mechanism of tumoritropic accumulation of proteins and the antitumor agent smancs, Canc. Res. 46 (12 Part 1) (1986) 6387–6392.
[18] A.L. Klibanov, K. Maruyama, V.P. Torchilin, L. Huang, Amphipathic polyethyleneglycols effectively prolong the circulation time of liposomes, FEBS (Fed. Eur. Biochem. Soc.) Lett. 268 (1) (1990) 235–237.
[19] J.D. Byrne, T. Betancourt, L. Brannon-Peppas, Active targeting schemes for nanoparticle systems in cancer therapeutics, Adv. Drug Deliv. Rev. 60 (15) (2008) 1615–1626.
[20] S.D. Steichen, M. Caldorera-Moore, N.A. Peppas, A review of current nanoparticle and targeting moieties for the delivery of cancer therapeutics, Eur. J.

Pharmaceut. Sci. 48 (3) (2013) 416–427.
[21] D.A. Christian, O.B. Garbuzenko, T. Minko, D.E. Discher, Polymer vesicles with a red cell-like surface charge: microvascular imaging and in vivo tracking with near-infrared fluorescence, Macromol. Rapid Commun. 31 (2) (2010) 135–141.
[22] D. Arcizet, B. Meier, E. Sackmann, J.O. Rädler, D. Heinrich, Temporal analysis of active and passive transport in living cells, Phys. Rev. Lett. 101 (24) (2008) 248103.
[23] C. Pelzl, D. Arcizet, G. Piontek, J. Schlegel, D. Heinrich, Axonal guidance by surface microstructuring for intracellular transport investigations, ChemPhysChem 10 (16) (2009) 2884–2890.
[24] A. Dupont, M. Gorelashvili, V. Schüller, F. Wehnekamp, D. Arcizet, Y. Katayama, D.C. Lamb, D. Heinrich, Three-dimensional single-particle tracking in live cells: news from the third dimension, N. J. Phys. 15 (7) (2013) 075008.
[25] N. Bossert, D. de Bruin, M. Götz, D. Bouwmeester, D. Heinrich, in: Fluorescence-tunable Ag-dna Biosensor with Tailored Cytotoxicity for Live-cell Applications, vol. 6, 2016, p. 37897.
[26] M. Camblin, P. Detampel, H. Kettiger, D. Wu, V. Balasubramanian, J. Huwyler, Polymersomes containing quantum dots for cellular imaging, Int. J. Nanomed. 9 (1) (2013) 2287–2298.
[27] G.-Y. Liu, C.-J. Chen, J. Ji, Biocompatible and biodegradable polymersomes as delivery vehicles in biomedical applications, Soft Matter 8 (34) (2012) 8811–8821.
[28] P.P. Ghoroghchian, M.J. Therien, D.A. Hammer, In vivo fluorescence imaging: a personal perspective, Wiley Interdisciplinary Reviews: Nanomedicine and Nanobiotechnology 1 (2) (2009) 156–167.
[29] D.H. Levine, P.P. Ghoroghchian, J. Freudenberg, G. Zhang, M.J. Therien, M.I. Greene, D.A. Hammer, R. Murali, Polymersomes: a new multi-functional tool for cancer diagnosis and therapy, Methods 46 (1) (2008) 25–32.
[30] N.A. Christian, M.C. Milone, S.S. Ranka, G. Li, P.R. Frail, K.P. Davis, F.S. Bates, M.J. Therien, P.P. Ghoroghchian, C.H. June, D.A. Hammer, Tat-functionalized near-infrared emissive polymersomes for dendritic cell labeling, Bioconjugate Chem. 18 (1) (2007) 31–40.
[31] L. Pourtau, H. Oliveira, J. Thevenot, Y. Wan, A.R. Brisson, O. Sandre, S. Miraux, E. Thiaudiere, S. Lecommandoux, Antibody-functionalized magnetic polymersomes: in vivo targeting and imaging of bone metastases using high resolution MRI, Advanced Healthcare Materials 2 (11) (2013) 1420–1424.
[32] W.-C. Huang, Y.-C. Chen, Y.-H. Hsu, W.-Y. Hsieh, H.-C. Chiu, Development of a diagnostic polymersome system for potential imaging delivery, Colloids Surfaces B Biointerfaces 128 (2015) 67–76.
[33] X. Tian, M.R. Gill , I. Cantón, J.A. Thomas, G. Battaglia, Live cell luminescence imaging as a function of delivery mechanism, Chembiochem 12 (4) (2011) 548–551.
[34] E. Scarpa, J.L. Bailey, A.A. Janeczek, P.S. Stumpf, A.H. Johnston, R.O.C. Oreffo, Y.L. Woo, Y.C. Cheong, N.D. Evans, T.A. Newman, in: Quantification of Intracellular Payload Release from Polymersome Nanoparticles, vol. 6, 2016, p. 29460.
[35] S.H.C. Askes, W. Pomp, S.L. Hopkins, A. Kros, S. Wu, T. Schmidt, S. Bonnet, Imaging upconverting polymersomes in cancer cells: biocompatible antioxidants brighten triplet-triplet annihilation upconversion, Small 12 (40) (2016) 5579–5590.
[36] J.E. Puskas, Y. Chen, Y. Dahman, D. Padavan, Polyisobutylene-based biomaterials, J. Polym. Sci. Polym. Chem. 42 (13) (2004) 3091–3109.
[37] A. Vonarbourg, C. Passirani, P. Saulnier, J.-P. Benoit, Parameters influencing the stealthiness of colloidal drug delivery systems, Biomaterials 27 (24) (2006) 4356–4373.
[38] S.R. Burks, E.A. Legenzov, E.W. Martin, C. Li, W. Lu, J.P.Y. Kao, Co-encapsulating the fusogenic peptide INF7 and molecular imaging probes in liposomes increases intracellular signal and probe retention, PLoS One 10 (3) (2015) e0120982.
[39] S.H.C. Askes, Upconverting Nanovesicles for the Activation of Ruthenium Anticancer Prodrugs with Red Light (Ph.D. thesis), Leiden University, Leiden, 2016, pp. 257–258 (Appendix VII).
[40] S. Sieber, P. Grossen, P. Detampel, S. Siegfried, D. Witzigmann, J. Huwyler, Zebrafish as an early stage screening tool to study the systemic circulation of nanoparticulate drug delivery systems in vivo, J. Contr. Release 264 (Supplement C) (2017) 180–191.
[41] J. Yang, Y. Shimada, R.C.L. Olsthoorn, B.E. Snaar-Jagalska, H.P. Spaink, A. Kros, Application of coiled coil peptides in liposomal anticancer drug delivery using a zebrafish xenograft model, ACS Nano 10 (8) (2016) 7428–7435.
[42] F. Campbell, F.L. Bos, S. Sieber, G. Arias-Alpizar, B.E. Koch, J. Huwyler, A. Kros, J. Bussmann, Directing nanoparticle biodistribution through evasion and exploitation of stab2-dependent nanoparticle uptake, ACS Nano 12 (2018) 2138–2150.
[43] Y.-Y. Won, A.K. Brannan, H.T. Davis, F.S. Bates, Cryogenic transmission electron microscopy (Cryo-TEM) of micelles and vesicles formed in water by poly(-ethylene oxide)-based block copolymers, J. Phys. Chem. B 106 (13) (2002) 3354–3364.
[44] D. Marsh, Handbook of Lipid Bilayers, second ed., Taylor & Francis Group, LLC, Boca Raton, FL, USA, 2013.
[45] S.L.H. Hopkins, B. Siewert, S.H.C. Askes, P. van Veldhuizen, R. Zwier, M. Heger, S. Bonnet, In vitro cell irradiation protocol for testing photopharmaceuticals and the effect of blue, green, and red light on human cancer cell lines, Photochem. Photobiol. Sci. 15 (5) (2016) 644–653.
[46] A.F. Gazdar, L. Girard, W.W. Lockwood, W.L. Lam, J.D. Minna, Lung cancer cell lines as tools for biomedical discovery and Research, JNCI (J. Natl. Cancer Inst.): J. Natl. Cancer Inst. (Bethesda) 102 (17) (2010) 1310–1321.
[47] M. Zanoni, F. Piccinini, C. Arienti, A. Zamagni, S. Santi, R. Polico, A. Bevilacqua, A. Tesei, 3D tumor spheroid models for in vitro therapeutic screening: a systematic approach to enhance the biological relevance of data obtained, Sci. Rep. 6 (2016) 19103.
[48] L.N. Lameijer, D. Ernst, S.L. Hopkins, M.S. Meijer, S.H.C. Askes, S.E. Le Dévédec, S. Bonnet, A red-light-activated ruthenium-caged NAMPT inhibitor remains phototoxic in hypoxic cancer cells, Angew. Chem. Int. Ed. 56 (38) (2017) 11549–11553.
[49] K.H. Bae, J.Y. Lee, S.H. Lee, T.G. Park, Y.S. Nam, Optically traceable solid lipid nanoparticles loaded with siRNA and paclitaxel for synergistic chemotherapy with in situ imaging, Advanced Healthcare Materials 2 (4) (2013) 576–584.
[50] J.A. Kim, C. Aberg, A. Salvati, K.A. Dawson, Role of cell cycle on the cellular uptake and dilution of nanoparticles in a cell population, Nat. Nanotechnol. 7 (1) (2012) 62–68.
[51] J. Rejman, A. Bragonzi, M. Conese, Role of clathrin- and caveolae-mediated endocytosis in gene transfer mediated by lipo- and polyplexes, Mol. Ther. 12 (3) (2005) 468–474.
[52] A.T. Jones, Macropinocytosis: searching for an endocytic identity and role in the uptake of cell penetrating peptides, J. Cell Mol. Med. 11 (4) (2007) 670–684.
[53] G. Sahay, D.Y. Alakhova, A.V. Kabanov, Endocytosis of nanomedicines, J. Contr. Release 145 (3) (2010) 182–195.
[54] S. Zhang, H. Gao, G. Bao, Physical principles of nanoparticle cellular endocytosis, ACS Nano 9 (9) (2015) 8655–8671.
[55] N. Oh, J.-H. Park, Endocytosis and exocytosis of nanoparticles in mammalian cells, Int. J. Nanomed. 9 (Suppl 1) (2014) 51–63.
[56] V. Vichai, K. Kirtikara, Sulforhodamine B colorimetric assay for cytotoxicity screening, Nat. Protoc. 1 (3) (2006) 1112–1116.
[57] J.-Y. Tinevez, N. Perry, J. Schindelin, G.M. Hoopes, G.D. Reynolds, E. Laplantine, S.Y. Bednarek, S.L. Shorte, K.W. Eliceiri, TrackMate: an open and extensible platform for single-particle tracking, Methods 115 (2016) 80–90, https://doi.org/10.1016/j.ymeth.2016.09.016.
[58] J. Schindelin, I. Arganda-Carreras, E. Frise, V. Kaynig, M. Longair, T. Pietzsch, S. Preibisch, C. Rueden, S. Saalfeld, B. Schmid, J.-Y. Tinevez, D.J. White, V. Hartenstein, K. Eliceiri, P. Tomancak, A. Cardona, Fiji: an open-source platform for biological-image analysis, Br. J. Pharmacol. 9 (7) (2012) 676–682.
[59] E. Granger, G. McNee, V. Allan, P. Woodman, The role of the cytoskeleton and molecular motors in endosomal dynamics, Semin. Cell Dev. Biol. 31 (2014) 20–29.
[60] H. Akita, K. Enoto, T. Masuda, H. Mizuguchi, T. Tani, H. Harashima, Particle tracking of intracellular trafficking of octaarginine-modified liposomes: a comparative study with adenovirus, Mol. Ther. 18 (5) (2010) 955–964.
[61] H. Li, Z.-W. Duan, P. Xie, Y.-R. Liu, W.-C. Wang, S.-X. Dou, P.-Y. Wang, Effects of paclitaxel on EGFR endocytic trafficking revealed using quantum dot tracking in single cells, PLoS One 7 (9) (2012) e45465.
[62] X. Nan, P.A. Sims, X.S. Xie, Organelle tracking in a living cell with microsecond time resolution and nanometer spatial precision, ChemPhysChem 9 (5) (2008) 707–712.
[63] X. Nan, P.A. Sims, P. Chen, X.S. Xie, Observation of individual microtubule motor steps in living cells with endocytosed quantum dots, J. Phys. Chem. B 109 (51) (2005) 24220–24224.
[64] I.R. Fernando, D.P. Ferris, M. Frasconi, D. Malin, E. Strekalova, M.D. Yilmaz, M.W. Ambrogio, M.M. Algaradah, M.P. Hong, X. Chen, M.S. Nassar, Y.Y. Botros, V.L. Cryns, J.F. Stoddart, Esterase- and pH-responsive poly([small beta]-amino ester)-capped mesoporous silica nanoparticles for drug delivery, Nanoscale 7 (16) (2015) 7178–7183.
[65] J. Schindelin, I. Arganda-Carreras, E. Frise, V. Kaynig, M. Longair, T. Pietzsch, S. Preibisch, C. Rueden, S. Saalfeld, B. Schmid, J.-Y. Tinevez, D.J. White, V. Hartenstein, K. Eliceiri, P. Tomancak, A. Cardona, Fiji: an open-source platform for biological-image analysis, Br. J. Pharmacol. 9 (7) (2012) 676–682.
[66] B.M. Weinstein, D.L. Stemple, W. Driever, M.C. Fishman, gridlock, a localized heritable vascular patterning defect in the zebrafish, Nat. Med. 1 (11) (1995) 1143–1147.